Efficient Emission in Halide Layered Double Perovskites: The Role of Sb^{3+} Substitution in $Cs_4Cd_{1-x}Mn_xBi_2Cl_{12}$ Phosphors

Brenda Vargas,[†] Eduardo Coutiño-Gonzalez,[⊥] Oscar Ovalle-Encinia,[‡] Citlali Sánchez-Aké,[▲] and Diego Solis-Ibarra[†]*

[†] Instituto de Investigaciones en Materiales, Universidad Nacional Autónoma de México, CU, Coyoacán, 04510, Ciudad de México, México
E-mail: diego.solis@unam.com

[⊥] Centro de Investigaciones en Óptica, A. C., Loma del Bosque 115, Colonia Lomas del Campestre, León, Guanajuato, 37150, México

[‡] School for Engineering of Matter, Transport and Energy, Arizona State University, Tempe, AZ 85260, USA

[▲] Instituto de Ciencias Aplicadas y Tecnología, Universidad Nacional Autónoma de México, CU, Coyoacán, 04510, Ciudad de México, México

ABSTRACT: Layered halide perovskites and double perovskites optoelectronic properties have recently been the subject of intense research. Layered double perovskites represent the merging of both worlds, and as such, have the potential to further expand the already vast space of optoelectronic properties and applications of halide perovskites. Despite having more than 40 known members, to date, only the <111>-oriented layered double perovskites: $Cs_4Cd_{1-x}Mn_x\mathbf{Bi}_2Cl_{12}$, have shown efficient photoluminescence (PL). In this work, we replaced Bi with Sb to further investigate the electronic structure and PL properties of these materials, resulting in two new families of layered inorganic perovskites alloys with full solubility. The first family, $Cs_4Cd_{1-x}Mn\mathbf{Sb}_2Cl_{12}$, exhibits a PL emission at 605 nm ascribed to Mn^{2+} centers in octahedral coordination, and a maximum photoluminescence quantum yield PLQY of 28.5%. The second family of alloys, also with full solubility, $Cs_4Cd_{0.8}Mn_{0.2}(\mathbf{Sb}_{1-y}\mathbf{Bi}_y)_2Cl_{12}$, contains a fixed amount of Mn^{2+} and Cd^{2+} cations but different concentrations of the trivalent metals. This variability allows the tuning of the PL emission from 603 nm to 614 nm. We show that the decreased efficiency of the $Cs_4Cd_{1-x}Mn_x\mathbf{Sb}_2Cl_{12}$family compared to $Cs_4Cd_{1-x}Mn_x\mathbf{Bi}_2Cl_{12}$, is mostly due to a decreased spin-orbit coupling in Sb and the subsequent increased electronic delocalization compared to the Bi alloys, reducing the energy transfer to Mn^{2+} centers. This work lays out a roadmap to understand and achieve high photoluminescence efficiencies in layered double perovskites.

The positioning of halide perovskites as the next high-performance semiconductors was possible thanks to their remarkable optoelectronic properties such as small bandgaps, disperse bands and weak exciton binding energies. Despite such benevolent properties, the toxicity of lead and long term-stability have raised some concerns.[1] An alternative to tackle the latter problem is to reduce the dimensionality of the perovskites by inserting hydrophobic cations that also modify the physical and electronic properties of the materials allowing a wider variety of compositions and properties.[2–4] An approach to tackle the toxicity of Pb is to replace it through an heterovalent substitution, which renders an elpasolite structure or double perovskite.[5] The combination of both strategies, dimensional reduction and heterovalent substitution, expands even further the already prolific halide perovskite realm. Further, structural and electronic dimensional reduction in these materials produces quantum confinement in bulk solids without the need of nanostructure synthesis protocols and, contrary to their 3D counterparts, they exhibit larger bandgaps, less dispersive bands and high exciton binding energies.[2,3,6] These properties have been exploited for luminescent applications in nonlinear optical processes,[7–9] LEDs,[10] among others.

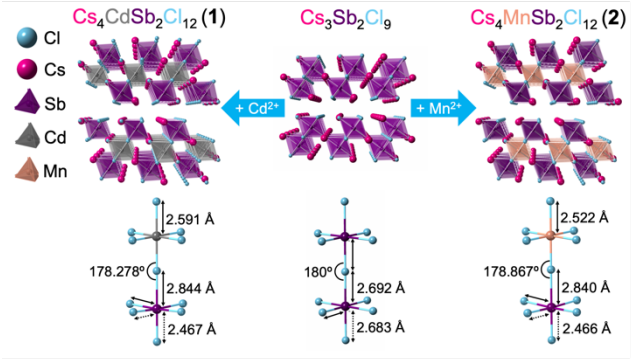

Figure 1. Top: crystal structures of $Cs_4CdSb_2Cl_{12}$, $Cs_3Sb_2Cl_9$, and $Cs_4MnSb_2Cl_{12}$. Bottom: the equatorial, axial bond lengths and Mn-Cl-Sb angle in the corresponding octahedra.

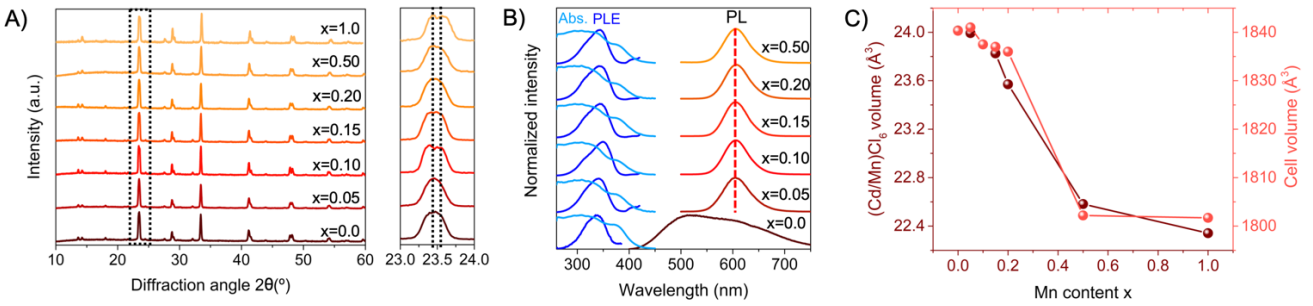

Figure 2. A) PXRD diffractograms of the $Cs_4Cd_{1-x}Mn_x\mathbf{Sb}_2Cl_{12}$ family of <111>-oriented layered perovskites with increasing Mn content x, and B) UV-Vis diffuse reflectance measurements converted to pseudo-absorbance, PL and PLE spectra for increasing Mn content, C) $(Cd/Mn)Cl_6$ and cell volumes decreased with increasing Mn content.

Conceptually, layered perovskites are derived by slicing the 3D framework in a crystallographic direction.[2] Experimentally, this can be achieved by incorporating a large organic cation that separates the inorganic layers or by replacing Pb^{2+} with a metal in a different oxidation state, such as Bi^{3+} or Sb^{3+}. The charge difference is compensated by the generation of ordered vacancies throughout the lattice, which results in a layered perovskite structure known as a <111>-oriented layered perovskite $A_3B^{III}{}_2X_9$.[11] The thickness of the inorganic sheets can be increased with a heterovalent replacement of the trivalent metal by two metals, M'^{II} and M^{III}, yielding the triple-layer structure $A_4M'^{II}M^{III}{}_2X_{12}$ (M = Bi^{3+}, Sb^{3+}; M' = Cd^{2+}, Mn^{2+}, Cu^{2+}) or a layered double perovskite, where one layer of $M'^{II}Cl_6$ octahedra alternates with two layers of $M^{III}Cl_6$ octahedra.[12] In Pb and Sn halide perovskites, the optical properties show a significant and systematic variation with the thickness of the sheet *n*.[13] In the <111>-oriented layered perovskites, *n* can be modulated by changing the metals in the structure. This metal substitution drastically changes the optical and electronic properties of the materials giving rise to a broad range of applications, from absorbers in solar cells,[12,14] phosphors,[15] photodetectors,[16–18] and spintronics.[19–21]

Recently, a new family of crystalline solid solutions was reported: $Cs_4Cd_{1-x}Mn_x\mathbf{Bi}_2Cl_{12}$ (x = 0 – 1), with a PL emission centered at 595 nm ascribed to the parity and spin forbidden $^4T_1(G) \rightarrow {}^6A_1(S)$ transition of octahedrally coordinated Mn^{2+} ions.[15] Later, we reported an improved PLQY of 79.5% with a Mn content of 10 % (x = 0.10), attributed to a favorable energy band alignment and the low dimensional nature of the perovskites that enhances an efficient energy transfer from the host to Mn^{2+} ions.[22] Woodward and coworkers proposed that the $[BiCl_6]^{3-}$ octahedra in the structure act as sensitizers that transfer the energy to Mn^{2+} recombination sites. The incorporation of Cd^{2+} electronically isolates Mn–Bi–Mn networks increasing radiative recombination in Mn^{2+} sites.[15] To date, this is the only family of layered double perovskites that displays efficient PLQY.[3,13,23]

The family of solid solutions $Cs_4Cd_{1-x}Mn_x\mathbf{Bi}_2Cl_{12}$, proved to be chemically stable with a highly efficient PL and interesting magnetic properties that could be harnessed in spin-electronics and spin-photonics applications.[20,24] Thus, we decided to explore the effects of substituting Bi by Sb in the materials optoelectronic properties. Herein, we report the optical and magnetic properties of a new family of solid solutions $Cs_4Cd_{1-x}Mn_x\mathbf{Sb}_2Cl_{12}$ with x spanning from 0 to 1.

The materials present a PL emission centered at 605 nm, ascribed to the Mn^{2+} centers, and a maximum PLQY of 28.5% for a Mn^{2+} content of 20 % (x = 0.20). The drop in PLQY, compared to the 78.5% PLQY in the Bi materials, results from a less efficient energy transfer from Sb sensitizers to Mn^{2+} activators mostly due to the decreased spin–orbit coupling in Sb and the increased electronic delocalization. We also report the synthesis of Sb-Bi alloys, $Cs_4Cd_{0.8}Mn_{0.2}(\mathbf{Sb}_{1-y}\mathbf{Bi}_y)_2Cl_{12}$, over the entire *y* composition range from 0 to 1. Furthermore, the mixed alloys allow the modulation of the PL emission maximum from 603 nm to 614 nm exhibiting a non–linear band gap variation that decreases the energy transfer to Mn^{2+} centers.

Replacing Bi^{3+} with Sb^{3+} in the solid solutions was the next natural step for several reasons: it allows to assess the role of the trivalent metal in the optical properties of the phosphors, expanding our understanding of the luminescent properties of layered double perovskites. Also, it is known that an efficient energy transfer from Sb^{3+} activators to Mn^{2+} sensitizers pairs can take place, which has been exploited in commercial phosphors such as $[3Ca_3(PO_4)_2Ca(F, Cl)_2 : Sb^{3+}, Mn^{2+}]$, and other host matrices.[25–27] Thus, Sb^{3+} substitution could potentially lead to an improved luminescence.

In a previous work, the end members of the new $Cs_4Cd_{1-x}Mn_x\mathbf{Sb}_2Cl_{12}$ family of solid solutions, $Cs_4Cd\mathbf{Sb}_2Cl_{12}$ (**1**) and $Cs_4Mn\mathbf{Sb}_2Cl_{12}$ (**2**), were prepared by precipitation of the respective metallic salts in concentrated hydrochloric acid.[28,29] Despite the ionic radii difference between Cd^{2+} and Mn^{2+}, both powders crystallize in the same trigonal $R\bar{3}m$ structure. As expected, the intermediate solid solutions can also be synthesized by this method (see SI) to obtain whitish powders with a light yellow or pink tone for the Mn-only compound. Analysis of powder X-ray diffraction (PXRD) data indicates that intermediate materials are pure and isostructural to the end members (Figure 2A). Mn is effectively incorporated in the structure as confirmed by the slight shift to higher diffraction angles that originates from the incorporation of the smaller cation Mn^{2+} in Cd^{2+} sites, and by the decrease of the cell and $(Cd_{1-x}/Mn_x)Cl_6$ octahedra volumes (Figure 2C), obtained from Rietveld refinements (Table S2). Inductively Couple Plasma-Optical Emission Spectroscopy (ICP-OES) analysis indicates that the nominal content of Mn almost perfectly matches the actual Mn^{2+} content in the samples (Table S2), allowing an optimal control of Mn incorporation in these materials.

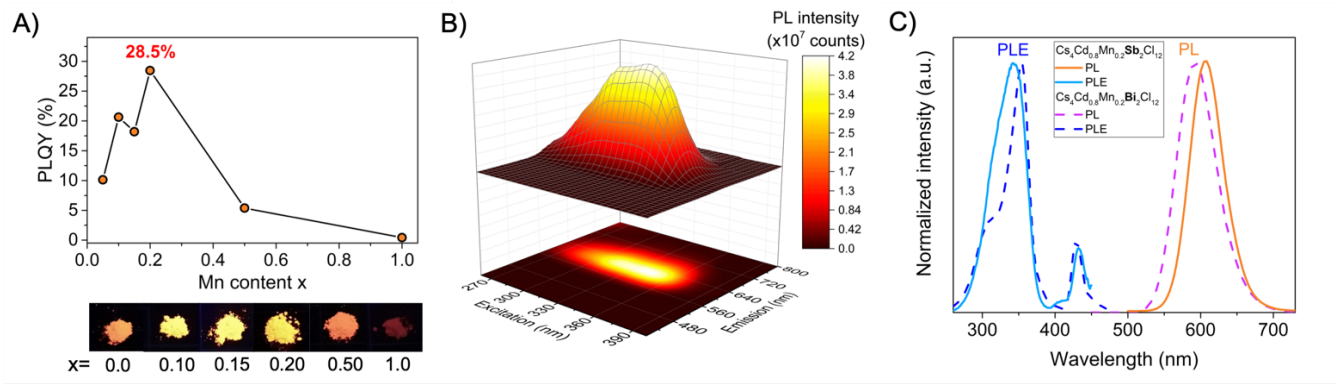

Figure 3. A) PLQY as a function of Mn^{2+} content for the family of materials $Cs_4Cd_{1-x}Mn_xSb_2Cl_{12}$, B) photo–excitation 3D mapping of $Cs_4Cd_{0.8}Mn_{0.2}Sb_2Cl_{12}$ and, C) comparison between PLE and PL spectra of $Cs_4Cd_{0.8}Mn_{0.2}Sb_2Cl_{12}$ and $Cs_4Cd_{0.8}Mn_{0.2}Bi_2Cl_{12}$.

Thermogravimetric analysis shows that the materials are stable up to 265°C (Figure S1).[28,29]

Distortions in the $M^{III}Cl_6$ octahedra can play an important role in these structures and a method to measure them is with the quadratic elongation and variance of octahedral angles (see Table S3).[30] The $SbCl_6$ octahedra in $Cs_3Sb_2Cl_9$ are almost perfect (Figure 1), only presenting a slight variance in the angle bond. However, a larger variance of the octahedral angles in the $M^{III}Cl_6$ octahedra was observed in the Cd–containing structures, $Cs_4CdSb_2Cl_{12}$ and $Cs_4CdBi_2Cl_{12}$ (Table S3). On the other hand, $MnCl_6$ and $CdCl_6$ form perfect octahedra in both structures, with bond lengths of Mn–Cl = 2.522 Å and Cd–Cl = 2.591 Å, respectively.

First, we analyzed the optical absorption of the samples with increasing Mn^{2+} content (Figure 2B). All samples display a single broad absorption band with a maximum at ~310 nm likely associated with the spin-forbidden $^1S_0 \rightarrow {}^3P_1$ transition of the $SbCl_6$ octahedra,[31,32] and an absorption edge that redshifts approximately 15 nm from the Cd–pure compound to the Mn–pure compound. Unlike their Bi^{3+} analogues, optical absorption from *d–d* Mn^{2+} transitions, $^4T_1(G) \rightarrow {}^6A_1(S)$ and $^4T_2(G) \rightarrow {}^6A_1(S)$, were not observed (see absorbance comparison of both families in Figure S4).

All Mn–containing materials present a PL emission centered at 606 nm with a FWHM of 58 nm with similar features and shapes (Figure 2B). The emission comes from the spin and parity forbidden $^4T_1(G) \rightarrow {}^6A_1(S)$ transition of Mn^{2+} ions in octahedral coordination.[33] The Mn^{2+} emission is slightly different from the emission of the Bi materials, which is centered at 595 nm (Figure 3C). The volume of the $MnCl_6$ octahedra in structure **2** is 21.38 $Å^3$ (Figure 1), which is slightly smaller than the same octahedra in the Bi materials (21.49 $Å^3$). As a consequence, the transition energy between the $^4T_1$ and $^6A_1$ levels decreases due to an increased crystal field strength and thus, shifts the emission to longer wavelengths.[34] The PL spectrum of structure **1** is quite different from the samples that contain Mn^{2+} (Figure 2B); the emission is very broad with a full width at half-maximum (FWHM) of 220 nm and very low intensity. This kind of emission has been ascribed to self-trapped excitons (STEs) in similar materials.[35] The maximum PLQY of 28.5% is reached at x = 0.20 (Figure 3A). This efficiency is higher than other Mn-doped double halide perovskites and in the same order as some Mn-doped layered halide perovskites.[36–39] The PL emissions with excitations wavelengths from 300 to 380 nm (Figure S2) and the photoexcitation 3D plot (Figure 3B, S8) indicate that the emission comes from the same excited level as all excitation wavelengths produce the same emission profile. Interestingly, the band at 440 nm corresponding to the $^6A_2(S) \rightarrow {}^4T_2(G)$ transition of Mn^{2+} ions in the PLE spectra does not appear in the absorption spectra (Figure 2B and Figure 3C). The PL and PLE features of Sb and Bi are very similar (Figure 3C) suggesting that the emission mechanism is very similar in both families of perovskites.

We studied the magnetic coupling in $Cs_4Cd_{1-x}Mn_xSb_2Cl_{12}$ with electron paramagnetic resonance (EPR). Generally, in this type of systems, one would expect that as Mn^{2+} concentration increases, the distance between neighboring Mn^{2+} ions decreases, allowing adjacent Mn^{2+} to become magnetically coupled with each other.[33] The EPR spectra for x < 0.50 (Figure 4A, S10) show two features: a hyperfine structure originating from the interaction between the spin (S = 5/2) of the unpaired 3d electrons and the I = 5/2 spin of the ^{55}Mn nucleus, generally assigned to Mn^{2+} isolated ions,[40] and a broad signal ascribed to coupled Mn^{2+} pairs.[33] This behavior is similar to that observed in Bi-materials, albeit with an apparent weaker magnetic coupling in the Sb-materials. The presence of isolated Mn^{2+} ions, and Mn–Mn pairs was confirmed by the time–resolved photoluminescence (TRPL) curves which can be fitted with a bi–exponential function for x < 0.5 and tri–exponential function for x = 0.50. From the fitting, two decay lifetimes were obtained, one in the tenth of μs, and the second in the order of ms, two order of magnitude slower (Figure 4B, S8 and Table S11). The slower decay lifetime is generally associated to isolated Mn^{2+} ions and the faster decay lifetime to Mn–Mn pairs as magnetic exchange relaxes the spin forbidden *d–d* transitions of Mn ions.[33] Further, for the Bi materials, the hyperfine structures are clearly visible only in the Mn–diluted regime (x = 0.005) (Figure S8), whereas for the Sb–materials, they are visible up to x = 0.15 despite having a shorter Mn–Mn bond length, 7.477 Å and 7.539 Å for neighboring Mn ions, respectively. This is further confirmed by the time–resolved PL emission measurements, where the exponential amplitudes or decay lifetimes with increasing Mn content up to x = 0.20 (Table S11 and Figures 4B, S8, S10) remain constant. It is also worth noting that the decay lifetime of isolated Mn^{2+} ions is three times larger than that of Bi–materials (see Table S12),

which also suggests a decreased exchange interaction between Mn^{2+} centers.

As predicted from theoretical calculations,[28] the band alignment changes depending on whether Sb or Bi is incorporated into these layered perovskites.[41] For example, a straightforward consequence of the trivalent metal substitution is that the Sb materials absorption edge is red shifted around 20 nm compared to Bi materials. However, the emission in Mn–doped materials is highly sensitive to the band edge position and band gap of the host, because both parameters affect the energy transfer to Mn^{2+} centers. Thus, we synthesized new solid solutions, $Cs_4Cd_{0.8}Mn_{0.2}(\mathbf{Sb}_{1-y}\mathbf{Bi}_y)_2Cl_{12}$ with different Bi contents (y), which turn out to have full Sb/Bi solubility in the 0 – 1 range. We decided to incorporate 80 % Cd content to increase the PL intensity as both, Bi and Sb materials, show high PL efficiency for this Cd/Mn ratio. This allowed us to tune the absorption band edge and to determine its effect on the energy transfer to Mn^{2+} ions. The PXRD patterns confirm single phases (Figure 5A). The absorbance spectra (Figure 5B) show that the doublet of the $^1S_0 \rightarrow {}^3P_1$ transition, which only appears in the Bi materials, emerges for a Bi content of $y > 0.9$ along with a visible increase in PL intensity (Figure 5D). Interestingly, the absorption band edge shifts to longer wavelengths until $y = 0.3$ and then shifts back to shorter wavelengths, a behavior known as band gap bowing (Figure 5B).[42,43] This is further corroborated by the yellow tone that the intermediate materials develop with changing concentrations of the trivalent metals. With the incorporation of small amounts of Bi in $Cs_4Cd_{0.8}Mn_{0.2}\mathbf{Sb}_2Cl_{12}$ ($y = 0$), the PL intensity drastically decreases (Figure S6), and the emission is shifted to shorter wavelengths from 614 to 603 nm as depicted in Figure 5C and 5D (see SI for more details on these measurements).

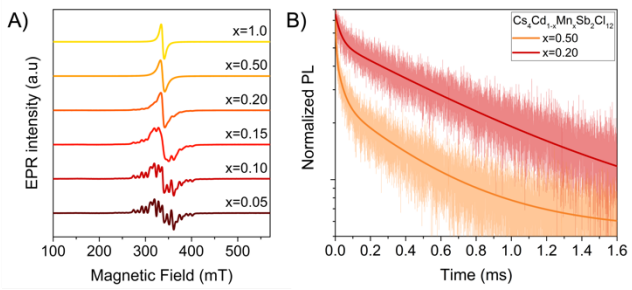

Figure 4. A) Room temperature electron paramagnetic resonance of $Cs_4Cd_{1-x}Mn_x\mathbf{Sb}_2Cl_{12}$ and B) time–resolved PL for x = 0. 20 and 0.50.

The replacement of Bi with Sb in the materials drastically affects the PLQY, since the Mn^{2+} emission depends on the energy transfer from the photo–excited host to the Mn^{2+} centers and the subsequent radiative decay from Mn^{2+} centers, one or perhaps both processes could be affected by the trivalent metal substitution. Several factors could be affecting the efficiency of the energy transfer from host to dopant, for instance, Woodward and coworkers propose that the Bi materials absorb light through localized excitations of the $BiCl_6$ octahedra and when returning to the ground state, they transfer the energy to the Mn^{2+} sites.[36] Delocalized wavefunctions yield dispersive bands and give rise to broad optical transitions, which accounts for the broadening of the doublet $^1S_0 \rightarrow {}^3P_1$ band in the absorption spectra with increasing Mn content in the Bi–materials (see SI).[13] The degeneracy of this spin–forbidden transition can be relaxed by spin–orbit coupling (SOC) and in some materials,[44] as $Cs_4Cd_{1-x}Mn_x\mathbf{Bi}_2Cl_{12}$ solid solutions, it can split into an asymmetric doublet resulting from a dynamic Jahn-Teller distortion. However, a single broad band is visible in the absorption spectra of $Cs_4Cd_{1-x}Mn_x\mathbf{Sb}_2Cl_{12}$, which suggests that the spin-orbit and/or the Jahn–Teller coupling in Sb ions is not as strong as in the Bi–materials. Interestingly, the crystal symmetry of both the Sb and Bi families is not affected by the dynamic Jahn Teller dynamic as both conserve the $R\bar{3}m$ crystal group. This dynamic expression of the ns^2 lone pair while maintaining the long-range symmetry has been reported for other double perovskites.[45] Since the SOC is not as strong in Sb, the spin–forbidden $^1S_0 \rightarrow {}^3P_1$ transitions cannot be relaxed, likely reducing the light absorption from the $SbCl_6$ octahedra.

As previously mentioned, the band alignment of the host has a critical role in the energy transfer to Mn^{2+} centers. The band gap nonlinearity or bowing in tin/lead perovskites has been attributed to the energy mismatch between atomic orbitals that compose the valence and conduction bands and also to a small contribution from lattice strain resulting in a band gap that becomes lower than either end compounds.[42] For $Cs_2Ag(Sb_xBi_{1-x})Br_6$ alloys, Z. Li and collaborators proposed a bowing originating from a type II gap alignment between the pure compounds, which allows the non–linear mixing of electronic states.[46] A similar effect could be taking place in the Bi/Sb solid solutions (Figure 5). Importantly, the band edge absorption shift has a clear effect on the PL intensity; as it shifts to shorter wavelengths, the emission intensity increases (Figure S6). Although the band edge shift does not behave linearly, it depicts the drastic effect that it has on the PL intensity and therefore on the energy transfer to Mn^{2+}. This result suggests that the substitution of Bi with Sb in the solid solutions is modifying the band alignment and decreasing the energy transfer to Mn^{2+} centers.

The decrease in PLQY is a consequence of the replacement of Bi orbitals with Sb orbitals in the band structure of these materials. DFT calculations of structures **1** and **2** were conducted in some previous work,[28,29,47] giving us insights into the electronic structure of these perovskites. The valence band maximum (VBM) is composed of Cd 4*d*/Cl 3*p* and Sb 5*s*/Cl 3*p* sates and the conduction band minimum (CBM) of Cd 5*s*/Cl 3*p* and Cl 3*p*/Sb 5*s* states. Furthermore, it is known that the 3*p* and 4*p* orbital overlap of halides in $Cs_4M^{2+}B^{3+}{}_2X_{12}$ is strong and that the *s* orbitals of the trivalent metals are significantly more delocalized than *d* orbitals leading to more dispersion in the valence band.[47] According to Woodward, in the Bi alloys, the incorporation of Cd^{2+} contributes to electronically isolate Mn–Bi–Mn networks by decreasing the electronic dimensionality of the structure and increasing radiative recombination on Mn^{2+} sites.[15] Furthermore, in some Bi materials, the relativistic contraction of the 6*s* orbital results in a more localized, lower-energy valence s orbital, compared to Sb 5*s* lone pair.[45,46,48] This is further supported by the fact that the Sb–materials band edge absorption is redshifted in comparison to the Bi–materials, which is an exception to the typical trend of decreasing bandgap upon atomic substitution with heavier members from the same

periodic group.[46] Hoye and collaborators observed the same effect in $Cs_2Ag(Sb_xBi_{1-x})Br_6$ alloys, which was attributed to a stronger interaction of the Sb $5s^2$ lone pair with Ag and Br orbitals. In our case, the band gap contraction could be due to a slight better coupling of the Sb lone pair with the Cl *p* and Cd orbitals that constitute both the CB and VB, slightly increasing delocalization but decreasing the radiative recombination on Mn^{2+} sites. It is worth noting that according to Xu et al., the Cd–materials exhibit an even parity in both the VBM and CBM so the optical transition between band edges are forbidden. This type of parity forbidden transitions can be partly allowed by distortions in the metal octahedra, which are slightly larger for the Bi materials (Table S3). This could also be a factor affecting light absorption by the trivalent metal. Overall, the replacement of Bi by Sb suggests a greater electronic delocalization likely reducing the radiative recombination at Mn^{2+} sites despite Cd^{2+} incorporation.

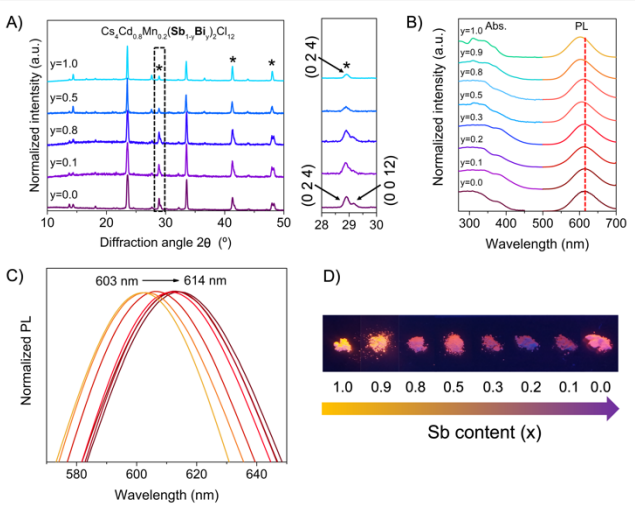

Figure 5. A) PXRD patterns of $Cs_4Cd_{0.8}Mn_{0.2}(\mathbf{Sb}_{1-y}\mathbf{Bi}_y)_2Cl_{12}$ solid solutions, the inset shows the doublet at 29° for y = 0 and the intensity decrease of the (0 0 12) diffraction peak. B) Absorbance and PL emission of $Cs_4Cd_{0.8}Mn_{0.2}(\mathbf{Sb}_{1-y}\mathbf{Bi}_y)_2Cl_{12}$ for $0 < y < 1$. C). Inset of PL emission spectra that shows the PL red–shift with increasing Sb content. D) Visual PL emission with increasing Sb content.

Another element that affects the efficiency of Mn^{2+} radiative decay is the magnetic exchange between Mn^{2+} centers. In general, the formation of Mn–Mn pairs is associated with the introduction of non–radiative recombination pathways that decrease the efficiency of Mn^{2+} radiative decay for large doping/substitution concentrations (known as concentration quenching), which explains the appearance of a third decay pathway in the TDPL spectra (Table 1). In the Bi materials, we proposed that the absorption bands corresponding to the spin and parity forbidden, $^6A_1(S) \rightarrow {}^4T_1(G)$ and $^6A_2(S) \rightarrow {}^4T_2(G)$ transitions, were partly allowed due to the magnetic coupling of Mn^{2+} pairs. In the Sb alloys, Mn^{2+} pairs are also magnetically coupled, as demonstrated by EPR results and previous susceptibility-temperature measurements that revealed an antiferromagnetic behavior in structure **2** (Figure 1),[29] but because the magnetic exchange is not as strong as in the Bi–materials, *d–d* transitions are absent in the absorption spectra. The Mn^{2+} concentration at which the maximum PLQY is attained (x = 0.10 for the Bi–materials, and x = 0.20 for the Sb–materials) differs because the magnetic exchange coupling between Mn centers in the Sb-materials is lower thus, non-recombination pathways appear for larger Mn concentrations than in the Bi–materials. In general, when Mn concentration increases the PL emission shifts to longer wavelengths due to magnetic interactions.[40] This is not the case for Sb materials, as PL emission remains constant at 605 nm throughout the entire range (Figure 2B). This is probably due to a long–range antiferromagnetic order via super–exchange interactions instead of a direct exchange coupling.[49]

In conclusion, we synthetized a new family of red-orange phosphors $Cs_4Cd_{1-x}Mn_x\mathbf{Sb}_2Cl_{12}$ with a maximum PLQY of 28.5%. We propose that the replacement of Bi orbitals by Sb orbitals in the valence and conduction bands improves orbital interaction which leads to electronic delocalization decreasing the energy transfer to Mn^{2+} centers. Further, the reduced SOC in Sb and the band realignment are also elements that affect the energy transfer to Mn^{2+} centers. We also demonstrated that metal alloying on the M^{3+} site is possible in these layered double perovskites, which allows further modulation of the optoelectronic properties. Overall, this work creates an opening to study the intriguing optoelectronic properties of this emerging family of layered double perovskites.

ASSOCIATED CONTENT

Supporting Information

The Supporting Information is available free of charge on the ACS Publications website.

Complete experimental details (PDF)

AUTHOR INFORMATION

Corresponding Author

*E-mail: diego.solis@unam.mx.

ORCID Diego Solis-Ibarra: 0000-0002-2486-0967

Funding Sources

The authors thank funding from PAPIIT IA202418 and CONACYT's CB-A1-S-8729 & CB-A1-S-44458.

ACKNOWLEDGEMENTS

We thank Carlos Ramos, Adriana Tejeda, Eriseth Morales, Lázaro Huerta, Alberto López, Alejandro Pompa, Cain González, Virginia Gómez and Miguel Angel Canseco for technical assistance. We also acknowledge M. Sc. Javier Tadeo Leon from the spectroscopy laboratory LANGEM-Instituto de Geología UNAM for the ICP analysis. B.V. acknowledges the support from CONACYT scholarship (Grant No. 270518).

REFERENCES

(1) Stoumpos, C. C.; Cao, D. H.; Clark, D. J.; Young, J.; Rondinelli, J. M.; Jang, J. I.; Hupp, J. T.; Kanatzidis, M. G. Ruddlesden-Popper Hybrid Lead Iodide Perovskite 2D Homologous Semiconductors. *Chem. Mater.* **2016**, *28*, 2852–2867.

(2) Smith, I. C.; Hoke, E. T.; Solis-Ibarra, D.; McGehee, M. D.; Karunadasa, H. I. A Layered Hybrid Perovskite Solar-Cell Absorber with Enhanced Moisture Stability. *Angew. Chemie - Int. Ed.* **2014**, *53*, 11232–11235.

(3) Connor, B. A.; Leppert, L.; Smith, M. D.; Neaton, J. B.; Karunadasa, H. I. Layered Halide Double Perovskites: Dimensional Reduction of $Cs_2AgBiBr_6$. *J. Am. Chem. Soc.* **2018**, *140*, 5235–5240.

(4) Ortiz-Cervantes, C.; Carmona-Monroy, P.; Solis-Ibarra, D. Two-Dimensional Halide Perovskites in Solar Cells: 2D or Not 2D? *ChemSusChem* **2019**, *12*, 1560–1575.

(5) Igbari, F.; Wang, Z. K.; Liao, L. S. Progress of Lead-Free Halide Double Perovskites. *Adv. Energy Mater.* **2019**, *9*, 1–32.

(6) Almutlaq, J.; Yin, J.; Mohammed, O. F.; Bakr, O. M. The Benefit and Challenges of Zero-Dimensional Perovskites. *J. Phys. Chem. Lett.* **2018**, *9*, 4131–4138.

(7) Trujillo-Hernández, K.; Rodríguez-López, G.; Espinosa-Roa, A.; González-Roque, J.; Gómora-Figueroa, A. P.; Zhang, W.; Halasyamani, P. S.; Jancik, V.; Gembicky, M.; Pirruccio, G.; Solis-Ibarra, D. Chirality Control in White-Light Emitting 2D Perovskites. *J. Mater. Chem. C* **2020**, *8*, 9602–9607.

(8) Xu, J.; Li, X.; Xiong, J.; Yuan, C.; Semin, S.; Rasing, T.; Bu, X. H. Halide Perovskites for Nonlinear Optics. *Adv. Mater.* **2020**, *32*, 1–13.

(9) Han, X.; Zheng, Y.; Chai, S.; Chen, S.; Xu, J. 2D Organic-Inorganic Hybrid Perovskite Materials for Nonlinear Optics. *Nanophotonics* **2020**, *9*, 1–24.

(10) Zhang, X.; Wang, C.; Zhang, Y.; Zhang, X.; Wang, S.; Lu, M.; Cui, H.; Kershaw, S. V.; Yu, W. W.; Rogach, A. L. Bright Orange Electroluminescence from Lead-Free Two-Dimensional Perovskites. *ACS Energy Lett.* **2019**, *4*, 242–248.

(11) Saparov, B.; Mitzi, D. B. Organic-Inorganic Perovskites: Structural Versatility for Functional Materials Design. *Chem. Rev.* **2016**, *116*, 4558–4596.

(12) Vargas, B.; Ramos, E.; Pérez-Gutiérrez, E.; Alonso, J. C.; Solis-Ibarra, D. A Direct Bandgap Copper-Antimony Halide Perovskite. *J. Am. Chem. Soc.* **2017**, *139*, 9116–9119.

(13) Connor, B. A.; Biega, R.-I.; Leppert, L.; Karunadasa, H. I. Dimensional Reduction of the Small-Bandgap Double Perovskite $Cs_2AgTlBr_6$. *Chem. Sci.* **2020**, *11*, 7708-7715.

(14) Saparov, B.; Hong, F.; Sun, J. P.; Duan, H. S.; Meng, W.; Cameron, S.; Hill, I. G.; Yan, Y.; Mitzi, D. B. Thin-Film Preparation and Characterization of $Cs_3Sb_2I_9$: A Lead-Free Layered Perovskite Semiconductor. *Chem. Mater.* **2015**, *27*, 5622–5632.

(15) Holzapfel, N. P.; Majher, J. D.; Strom, T. A.; Moore, C. E.; Woodward, P. M. $Cs4Cd_{1-x}MnxBi_2Cl_{12}$—A Vacancy-Ordered Halide Perovskite Phosphor with High-Efficiency Orange-Red Emission. *Chem. Mater.* **2020**, *32*, 3510–3516.

(16) Cai, T.; Shi, W.; Hwang, S.; Kobbekaduwa, K.; Nagaoka, Y.; Yang, H.; Hills-kimball, K.; Zhu, H.; Wang, J.; Wang, Z.; Liu, Y.; Su, D.; Gao, J.; Chen, O. Lead-Free $Cs_4CuSb_2Cl_{12}$ Layered Double Perovskite Nanocrystals. *J. Am. Chem. Soc.* **2020**, *142*, 11927–11936.

(17) Jayasankar, P. M.; Pathak, A. K.; Madhusudanan, S. P.; Murali, S.; Batabyal, S. K. Double Perovskite $Cs_4CuSb_2Cl_{12}$ Microcrystalline Device for Cost Effective Photodetector Applications. *Mater. Lett.* **2020**, *263*, 127200.

(18) Wang, X. D.; Miao, N. H.; Liao, J. F.; Li, W. Q.; Xie, Y.; Chen, J.; Sun, Z. M.; Chen, H. Y.; Kuang, D. Bin. The Top-down Synthesis of Single-Layered $Cs_4CuSb_2Cl_{12}$ Halide Perovskite Nanocrystals for Photoelectrochemical Application. *Nanoscale* **2019**, *11*, 5180–5187.

(19) Han, D.; Zhang, T.; Chen, S. High-Throughput First-Principles Screening of Layered Magnetic Double Perovskites $Cs_4MSb_2X_{12}$ for Spintronic Applications. *J. Phys. Condens. Matter* **2019**, *32*, 0–27.

(20) Tran, T. T.; Pocs, C. A.; Zhang, Y.; Winiarski, M. J.; Sun, J.; Lee, M.; Mcqueen, T. M.; Nat, O. R. Spinon Excitations in the Quasi-1D S = ½ Chain $Cs_4CuSb_2Cl_{12}$. *Phys. Rev. B* **2020**, *101*, 235107.

(21) Singhal, N.; Chakraborty, R.; Ghosh, P.; Nag, A. Low-Bandgap $Cs_4CuSb_2Cl_{12}$ Layered Double Perovskite: Synthesis, Reversible Thermal Changes, and Magnetic Interaction. *Chem. - An Asian J.* **2018**, *13*, 2085–2092.

(22) Vargas, B.; Reyes-Castillo, D. T.; Coutino-Gonzalez, E.; Ramos, C.; Sánchez-Aké, C.; Ciro, F.; Solis-Ibarra, D. Enhanced Luminescence and Mechanistic Studies on Mn-Doped Double Layered Perovskite Phosphors: $Cs_4Mn_{1-x}Cd_xBi_2Cl_{12}$. *ChemRxiv* **2020**.

(23) Jana, M. K.; Janke, S. M.; Dirkes, D. J.; Dovletgeldi, S.; Liu, C.; Qin, X.; Gundogdu, K.; You, W.; Blum, V.; Mitzi, D. B. Direct-Bandgap 2D Silver-Bismuth Iodide Double Perovskite: The Structure-Directing Influence of an Oligothiophene Spacer Cation. *J. Am. Chem. Soc.* **2019**, *141*, 7955–7964.

(24) Beaulac, R.; Archer, P. I.; Ochsenbein, S. T.; Gamelin, D. R. Mn^{2+}–Doped CdSe Quantum Dots: New Inorganic Materials for Spin-Electronics and Spin-Photonics. *Adv. Funct. Mater.* **2008**, *18*, 3873–3891.

(25) *Solid State Luminescence*, First edit.; Kitai, A. H., Ed.; Springer-Science+Business Media, B.V., 1993; Vol. 548.

(26) Chen, L.; Deng, X.; Xue, S.; Bahader, A.; Zhao, E.; Mu, Y.; Tian, H.; Lü, S.; Yu, K.; Jiang, Y.; Chen, S.; Tao, Y.; Zhang, W. The Energy Transfer in the Sb^{3+} and Eu^{3+} Co-Activated YBO_3 Phosphor and Their White Luminescence for Deep Ultraviolet LEDs Application. *J. Lumin.* **2014**, *149*, 144–149.

(27) Blasse, G.; Bril, A. Study of Energy Transfer from Sb^{3+}, Bi^{3+}, Ce^{3+} to Sm^{3+}, Eu^{3+}, Tb^{3+}, Dy^{3+}. *J. Chem. Phys.* **1967**, *47*, 1920–1926.

(28) Vargas, B.; Torres-Cadena, R.; Reyes-Castillo, D. T.; Rodríguez-Hernández, J.; Gembicky, M.; Menéndez-Proupin, E.; Solis-Ibarra, D. Chemical Diversity in Lead-Free, Layered Double Perovskites: A Combined Experimental and Computational Approach. *Chem. Mater.* **2020**, *32*, 424–429.

(29) Vargas, B.; Torres-Cadena, R.; Rodríguez-Hernández, J.; Gembicky, M.; Xie, H.; Jiménez-Mier, J.; Liu, Y. S.; Menéndez-Proupin, E.; Dunbar, K. R.; Lopez, N.; Olalde-Velasco, P.; Solis-Ibarra, D. Optical, Electronic, and Magnetic Engineering of <111> Layered Halide Perovskites. *Chem. Mater.* **2018**, *30*, 5315–5321.

(30) Robinson, K.; Gibbs, G. V.; Ribbe, P. H. Quadratic Elongation: A Quantitative Measure of Distortion in Coordination Polyhedra. *Science* **1971**, *172*, 567–570.

(31) Oomen, E. W. J. L.; Smit, W. M. A.; Blasse, G. On the Luminescence of Sb^{3+} in Cs_2NaMCl_6 (with M = Sc , Y , La): A Model System for the Sutdy of Trivalent s^2 Ions. *J. Phys. C Solid State Phys.* **1986**, *19*, 3263–3272.

(32) Li, J.; Tan, Z.; Hu, M.; Chen, C.; Luo, J.; Li, S.; Gao, L.; Xiao, Z.; Niu, G.; Tang, J. Antimony Doped Cs_2SnCl_6 with Bright and Stable Emission. *Front. Optoelectron.* **2019**, *12*, 352–364.

(33) Yang, X.; Pu, C.; Qin, H.; Liu, S.; Xu, Z.; Peng, X. Temperature- and Mn^{2+} Concentration-Dependent Emission Properties of Mn^{2+}–Doped ZnSe Nanocrystals. *J. Am. Chem. Soc.* **2019**, *141*, 2288–2298.

(34) *Fundamentals of Phosphors*; William, M. Y., Shionoya, S., Yamamoto, H., Eds.; CRC Press, 2007.

(35) McCall, K. M.; Stoumpos, C. C.; Kostina, S. S.; Kanatzidis, M. G.; Wessels, B. W. Strong Electron-Phonon Coupling and Self-Trapped Excitons in the Defect Halide Perovskites $A_3M_2I_9$ (A = Cs, Rb; M = Bi, Sb). *Chem. Mater.* **2017**, *29*, 4129–4145.

(36) Majher, J. D.; Gray, M. B.; Strom, T. A.; Woodward, P. M. $Cs_2NaBiCl_6$:Mn^{2+}–A New Orange-Red Halide Double Perovskite Phosphor. *Chem. Mater.* **2019**, *31*, 1738–1744.

(37) Nandha K, N.; Nag, A. Synthesis and Luminiscence of Mn-Doped $Cs_2AgInCl_6$ Double Perovskite. *ChemComm* **2018**, *54*, 5205–5208.

(38) Cortecchia, D.; Mróz, W.; Neutzner, S.; Borzda, T.; Folpini, G.; Brescia, R.; Petrozza, A. Defect Engineering in 2D Perovskite by Mn(II) Doping for Light-Emitting Applications. *Chem* **2019**, *5*, 2146–2158.

(39) Locardi, F.; Cirignano, M.; Baranov, D.; Dang, Z.; Prato, M.;

Drago, F.; Ferretti, M.; Pinchetti, V.; Fanciulli, M.; Brovelli, S.; De Trizio, L.; Manna, L. Colloidal Synthesis of Double Perovskite $Cs_2AgInCl_6$ and Mn-Doped $Cs_2AgInCl_6$ Nanocrystals. *J. Am. Chem. Soc.* **2018**, *140*, 12989–12995.

(40) Lin, J.; Zhang, Q.; Wang, L.; Liu, X.; Yan, W.; Wu, T.; Bu, X.; Feng, P. Atomically Precise Doping of Monomanganese Ion into Coreless Supertetrahedral Chalcogenide Nanocluster Inducing Unusual Red Shift in Mn^{2+} Emission. *J. Am. Chem. Soc.* **2014**, *136*, 4769–4779.

(41) Lin, Y.-P.; Hu, S.; Xia, B.; Fan, K.-Q.; Gong, L.-K.; Kong, J.-T.; Huang, X.-Y.; Xiao, Z.; Du, K.-Z. Material Design and Optoelectronic Properties of Three-Dimensional Quadruple Perovskite Halides. *J. Phys. Chem. Lett.* **2019**, *10*, 5219–5225.

(42) Goyal, A.; McKechnie, S.; Pashov, D.; Tumas, W.; Schilfgaarde, M. Van; Stevanović, V. Origin of Pronounced Nonlinear Band Gap Behavior in Lead-Tin Hybrid Perovskite Alloys. *Chem. Mater.* **2018**, *30*, 3920–3928.

(43) Du, K. Z.; Meng, W.; Wang, X.; Yan, Y.; Mitzi, D. B. Bandgap Engineering of Lead-Free Double Perovskite $Cs_2AgBiBr_6$ through Trivalent Metal Alloying. *Angew. Chemie - Int. Ed.* **2017**, *56*, 8158–8162.

(44) Polák, K.; Mihóková, E. In^{+}, Pb^{2+} and Bi^{3+} in KBr Crystal: Luminescence Dynamics. *Opt. Mater. (Amst).* **2010**, *32*, 1280–1282.

(45) Mccall, K. M.; Morad, V.; Benin, B. M.; Kovalenko, M. V. Efficient Lone Pair-Driven Luminescence: Structure-Property Relationships in Emissive $5s^2$ Metal Halides. *ACS Mater. Lett.* **2020**, *2*, 1218–1232.

(46) Li, Z.; Napari, M.; Palgrave, R. G.; Abdi-jalebi, M.; Andaji-garmaroudi, Z.; Davies, D. W.; Laitinen, M.; Julin, J.; Richard, H.; Scanlon, D. O.; Walsh, A.; Hoye, R. L. Z. Bandgap Lowering in Mixed Alloys of $Cs_2Ag(Sb_xBi_{1-x})Br_6$ Double Perovskite Thin Films. *arXiv:2007.00388 [cond-mat.mtrl-sci]* **2020**, 1–29.

(47) Xu, J.; Liu, J.-B.; Wang, J.; Liu, B.-X.; Huang, B. Prediction of Novel *p* -Type Transparent Conductors in Layered Double Perovskites: A First-Principles Study. *Adv. Funct. Mater.* **2018**, *28*, 1800332.

(48) Pyykkö, P. Relativistic Effects in Structural Chemistry. *Chem. Rev.* **1988**, *88*, 563–594.

(49) Xu, J.; Xu, C.; Liu, J.-B. Prediction of Room-Temperature Half-Metallicity in Layered Halide Double Perovskites. *npj Comput. Mater.* **2019**, 114.